



**HAL**  
open science

# Review of Rare-Earth Phosphate Materials for Nuclear Waste Sequestration Applications

Mohamed Ruwaid Rafiuddin, Giovanni Donato, Sarah Mccaugherty, Adel Mesbah, Andrew P. Grosvenor

► **To cite this version:**

Mohamed Ruwaid Rafiuddin, Giovanni Donato, Sarah Mccaugherty, Adel Mesbah, Andrew P. Grosvenor. Review of Rare-Earth Phosphate Materials for Nuclear Waste Sequestration Applications. ACS Omega, 2022, 7 (44), pp.39482-39490. 10.1021/acsomega.2c03271 . hal-03852368

**HAL Id: hal-03852368**

**<https://hal.science/hal-03852368>**

Submitted on 24 Nov 2022

**HAL** is a multi-disciplinary open access archive for the deposit and dissemination of scientific research documents, whether they are published or not. The documents may come from teaching and research institutions in France or abroad, or from public or private research centers.

L'archive ouverte pluridisciplinaire **HAL**, est destinée au dépôt et à la diffusion de documents scientifiques de niveau recherche, publiés ou non, émanant des établissements d'enseignement et de recherche français ou étrangers, des laboratoires publics ou privés.



Distributed under a Creative Commons Attribution - NonCommercial - NoDerivatives 4.0 International License

# **A review of rare-earth phosphate materials for nuclear waste sequestration applications**

Mohamed Ruwaid Rafiuddin<sup>1,2</sup>, Giovanni Donato<sup>1</sup>, Sarah McCaugherty<sup>1</sup>, Adel Mesbah<sup>3</sup>,  
Andrew P. Grosvenor<sup>1\*</sup>

<sup>1</sup>*Department of Chemistry, University of Saskatchewan, Saskatoon, SK, S7N 5C9*

<sup>2</sup>*MIAMI Irradiation Facility, School of Computing and Engineering, University of Huddersfield,  
HD1 3DH, UK*

<sup>3</sup>*Univ Lyon, Université Lyon 1, Institut de Recherches sur la Catalyse et l'Environnement de  
Lyon, IRCELYON, UMR5256, CNRS, 2 Avenue Albert Einstein, 69626, Villeurbanne Cedex,  
France*

## **Author Bios:**

Mohamed Ruwaid Rafiuddin: Dr. M. R. Rafiuddin earned his M.Sc. degree in Chemistry from the Indian Institute of Technology (IIT), Madras, India. He obtained his Ph.D. degree in Chemistry from the University of Saskatchewan, Canada and his thesis was focussed on the synthesis of rare-earth phosphate based nuclear waste forms and investigating the effect of radiation and corrosion on the structure of these waste forms. Following the completion of his Ph.D., Dr. Rafiuddin worked as a CNRS Postdoctoral Researcher at the Interface of Materials in Evolution Laboratory (LIME), Marcoule Institute for Separation Chemistry (ICSM), France. Dr. M. R. Rafiuddin currently works as a Research Fellow at the Microscope and Ion Accelerator for Materials Investigation (MIAMI), University of Huddersfield and his research interests include investigating the effect of ion radiation on ceramic and glass-ceramic wasteforms using in-situ TEM.

Giovanni Donato: Mr. Donato earned his B.Sc. degree from Toronto Memorial University (formally Ryerson University) and his M.Sc. degree from the University of Saskatchewan. The focus of Mr. Donato's M.Sc. thesis research was on the synthesis of and characterization of rare-earth phosphate containing glass-ceramic composite materials.

Sarah McCaugherty: Ms. McCaugherty earned her B.Sc. degree from the University of Waterloo and her M.Sc. degree from the University of Saskatchewan. The focus of Ms. McCaugherty's M.Sc. thesis research was on the synthesis of pyrochlore- and zirconolite-type oxides at temperatures lower than normally reported in the literature. Both oxide structures are popular materials for the proposed sequestration of actinide elements.

Adel Mesbah: Dr. Adel Mesbah is a CNRS researcher at IRCELYON in France. He earned his PhD at the University of Nancy I -Henri-Poincaré in France. Upon completion of his Ph.D., Dr.

Adel Mesbah worked as a postdoctoral researcher at the CEA Marcoule, ICSM, and at Northwestern University. In 2012, he joined the CNRS and worked at the ICSM Marcoule on topics related to the nuclear fuel cycle. In 2021, he joined IRCELYON, and his current research interests include studying materials for sustainable and affordable energy production.

Andrew P. Grosvenor: Prof. A. P. Grosvenor is a professor in the Department of Chemistry, University of Saskatchewan. He earned his B.Sc. and M.Sc. degrees from the University of Western Ontario and his Ph.D. from the University of Alberta. Following completion of his Ph.D., he was an NSERC Postdoctoral Fellow at McMaster University. The focus of Prof. Grosvenor's research program, which began in 2009, is the development and study of various materials for the safe sequestration of nuclear waste.

**Abstract:**

Several materials have or are currently being investigated for nuclear waste sequestration applications, including: crystalline ceramic oxides; glasses; and glass-ceramic composites. Rare-earth phosphates have been investigated extensively for this application owing to the range of structures that the hydrous or anhydrous versions can adopt as well as the fact that naturally occurring rare-earth phosphates have been found to contain U or Th. The purpose of this review is to discuss (generally) the properties that must be considered when identifying nuclear waste form materials and (more specifically) the structure and properties of rare-earth phosphates with special attention being given to the resistance of these materials to radiation-induced structure damage. The last section of the review contains an introduction to the development of glass-ceramic composite materials that contain rare-earth phosphate crystallites dispersed in a glass matrix. These composite materials have been suggested to be superior to using just glass or ceramic materials for nuclear waste sequestration applications owing to improved waste loading capabilities.

\*Corresponding author:  
Prof. Andrew P. Grosvenor  
[andrew.grosvenor@usask.ca](mailto:andrew.grosvenor@usask.ca)

## 1. Introduction:

Nuclear power is a major source of electricity worldwide.<sup>1</sup> As of 2017, there were 449 operable reactors which were responsible for generating 10.6% of the world's electricity.<sup>1</sup> With 55 reactors under construction, 111 ordered, and 328 proposed, the global nuclear industry is expanding.<sup>1</sup> In 2008, the International Energy Agency (IEA) projected that world energy requirements will nearly double by 2030.<sup>2</sup> Various "green" energy sources such as wind, solar, and nuclear have been proposed to meet these energy demands while combatting the prospect of climate change by producing little to no CO<sub>2</sub> emissions.<sup>1</sup> Intermittent sources of energy, like solar and wind energy, would rely on backup sources approximately 80% of the time, whereas nuclear power is available on a consistent basis.<sup>1</sup> Reliance on nuclear power provides energy security as the fuel is available from many politically stable countries, and the high energy density of uranium allows for easier storage of large energy reserves when compared to fossil fuels.<sup>1</sup> One disadvantage of nuclear power is the generation of nuclear (radioactive) waste.

Radioactive waste in Canada (for example) is generated from: uranium mining, milling, and refining; nuclear fuel fabrication; nuclear reactors; nuclear research; and radioisotope manufacturing and use.<sup>1</sup> This waste is categorized depending on the level of radioactivity detected and/or the heat emitted by the material.<sup>3</sup> Low-level radioactive waste (LLW) are those materials that are used in the workplace surrounding the use of radioactive materials (e.g. gloves, cloths, protective clothing).<sup>3</sup> Intermediate-level radioactive waste (ILW) has had more direct contact with radioactive materials, such as ion-exchange resins and reactor components.<sup>3</sup> High-level radioactive waste (HLW) is defined as spent fuel and other materials emitting >2 kW/m<sup>3</sup> of heat.<sup>3</sup> A waste form is defined as "waste in its physical and chemical form after treatment and/or conditioning (resulting in a solid product) prior to packaging".<sup>4</sup> The ultimate purpose of radioactive waste management is to immobilize radioactive elements in waste forms to prevent the release of those radionuclides into the environment.<sup>5</sup> Groundwater leaching has been identified as the most likely mechanism by which release of radionuclides may occur.<sup>4</sup> Therefore, the most important requirement for a waste form is to be chemically durable.<sup>4</sup> Additionally, an ideal waste form should be resistant to damage caused by radioactive decay processes, incorporate a wide range of elements with high loading, and be easy to fabricate with reasonable synthesis conditions.<sup>4,5</sup> Several types of waste forms have been studied to date including glasses, ceramics, and glass-ceramic composites. The purpose of this review is to discuss some of the waste form materials that have

been proposed for nuclear waste sequestration with specific attention being given to rare-earth phosphate-based waste form materials.

## **2. Types of nuclear waste form materials:**

### **2.1 Glasses:**

Radioactive glass waste forms were first produced via vitrification on an industrial scale at the AVM (*Atelier de Vitrification de Marcoule*) plant in Marcoule, France in 1978.<sup>6</sup> Since then, a global consensus has been reached on using glass materials, notably borosilicate glasses, as a host matrix for the immobilization of liquid HLW.<sup>5</sup> Currently, glass vitrification technology has been used in most countries for the conversion of liquid HLW into durable solid wastefoms.<sup>5</sup> The liquid HLWs which are compositionally diverse (i.e., contains a wide range of radionuclides) are homogenously distributed inside a glass matrix.<sup>5</sup> Borosilicate glasses that are being used worldwide as a HLW matrix are generally prepared using varying mass percentages of chemicals such as SiO<sub>2</sub>, B<sub>2</sub>O<sub>3</sub>, Al<sub>2</sub>O<sub>3</sub>, CaO, MgO, and Na<sub>2</sub>O. The waste loading capabilities of these glasses could range anywhere between 25% to 35% by mass.<sup>5,6</sup> In addition to borosilicate glass materials, other materials such as aluminophosphate-, silicate-, rare-earth oxide-, and iron-phosphate-glasses are also being considered for the immobilization of HLW.<sup>6</sup>

### **2.2 Ceramics:**

Naturally occurring crystalline minerals containing radionuclides are known to be on Earth for millions of years and have been exposed to extreme environmental conditions.<sup>7</sup> Some of the natural minerals have endured these extreme conditions and remained structurally stable on a geological timescale.<sup>7</sup> This observation has inspired scientists to propose synthetic analogues of these crystalline minerals for HLW immobilization applications.<sup>7</sup> Crystalline materials, unlike their amorphous counterparts (e.g., glasses), are thermodynamically stable and therefore should possess greater structural stability and chemical durability over long periods of time required for HLW storage.<sup>8</sup> In a crystalline waste form, the radionuclides occupy specific atomic sites of the host matrix and become a part of the crystal structure.<sup>7,8</sup> Since the atomic sites in a crystal structure have specific size, charge, and bonding requirements, the crystalline host matrix imposes restriction on the type of radioactive element that can be incorporated into the crystal structure.<sup>7,8</sup> As a result, different crystalline materials are being developed or proposed to host specific types of radioactive elements (e.g., fission products; minor actinides) that are present in liquid HLW.<sup>7,8</sup>

Among the various crystalline waste forms that have been studied, multiphase waste forms called SYNROC (synthetic rock) developed by Ringwood and coworkers have been investigated extensively in the literature.<sup>8</sup> SYNROC is a polyphase assemblage of synthetic analogues of Ti-containing crystalline minerals and generally comprise of hollandite ( $\text{BaAl}_2\text{Ti}_2\text{O}_6$ ), perovskite ( $\text{CaTiO}_3$ ), zirconolite ( $\text{CaZrTi}_2\text{O}_7$ ), and rutile ( $\text{TiO}_2$ ) phases.<sup>8</sup> The minerals constituting the SYNROC waste form have survived in various geological environments for millions of years and, therefore, SYNROC waste forms possess higher chemical durability than glass based wasteforms.<sup>8</sup> In addition to high durability, the presence of multiple crystalline phases in SYNROC also allows for the incorporation of a wide variety of radionuclides resulting from the reprocessing of spent fuel.<sup>8</sup> Single phase waste forms, on the other hand, are tailored for hosting specific radionuclides and some of the proposed crystalline waste forms include monazite ( $\text{CePO}_4$ ), xenotime ( $\text{YPO}_4$ ), brannerite ( $\text{UTi}_2\text{O}_6$ ), pyrochlore ( $\text{Gd}_2\text{Ti}_2\text{O}_7$ ), and zircon ( $\text{ZrSiO}_4$ ).<sup>7</sup> The leaching resistance of a material is one important property to consider when selecting materials as a nuclear waste form. It has been demonstrated that several crystalline ceramic phases have significantly improved resistance to leaching, as shown in **Figure 1**, as well as other properties that are beneficial to the implementation of these materials as nuclear waste forms.<sup>5,7</sup>

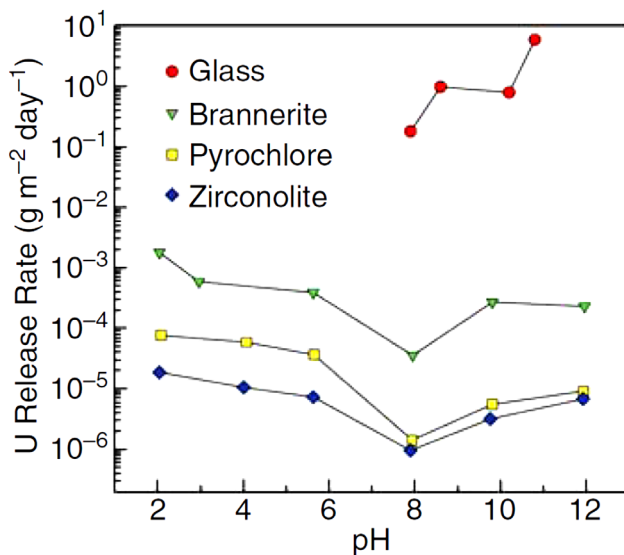


**Figure 1** Comparison of the U leach rate from glass, brannerite, pyrochlore, and zirconolite materials, demonstrating the increased chemical durability of ceramic materials relative to glass. Reprinted with permission from Reference <sup>7</sup> (Weber et al. *MRS Bull.* **2009**, 34, 46-53). Copyright 2009 Materials Research Society..<sup>7</sup>

### 2.3 Glass-ceramic composites:

Glass-ceramic composites, which may also be referred to as glass-crystalline materials or glass-composite materials, are heterogeneous materials that consist of ceramic crystallites dispersed in a glass matrix.<sup>9</sup> By synthesizing a material that contains both crystalline ceramic and amorphous glass, the final material can possess properties that are greater than the sum of its parts.<sup>10</sup> Various glass-ceramic composite materials have been investigated as waste forms for nuclear waste sequestration. These materials have been studied for a variety of reasons including that: 1) these materials have a higher waste loading of large elements (e.g., actinides) compared to glasses as these elements can be incorporated into specific crystallographic sites that are large enough to accommodate them; 2) the combination of both materials allows for all of the elements found in spent nuclear fuel to be accommodated either in the glass matrix or the crystalline ceramic; and 3) the glass surrounding the ceramic crystallites can act as a secondary barrier to restrict the crystallites being exposed to groundwater.<sup>9</sup>

### **3. Radiation effects in nuclear waste forms**

The radiation emanating from HLW is a result of radioactive decay of fission products (e.g., <sup>137</sup>Cs and <sup>90</sup>Sr) and minor actinides (e.g., Np, Am, Cm) present in the HLW stream.<sup>8</sup> The fission products decay via emission of  $\beta$  ( $e^-$ ) particles and in this process low-energy recoil nuclei, also called daughter products, are produced.<sup>8</sup> The minor actinides, on the other hand, decay by producing energetic  $\alpha$  ( $He^{2+}$ ) particles and high-energy recoil nuclei.<sup>8</sup> The fission products and minor actinides have shorter and longer half-lives, respectively.<sup>8</sup> As a result, for the first ~500 years of HLW storage, the radiation will predominantly arise from the  $\beta$ -decay of fission products after which the radiation will arise primarily from the  $\alpha$ -decay of actinides.<sup>7,8</sup> When these radionuclides are atomically confined within a solid matrix, the radioactive decay products dissipate their energy into the host matrix via ionization and elastic collision events.<sup>8</sup> In the case of an ionization event, the energies of the decay products are used to excite and remove electrons from the atoms in the solid whereas in an elastic collision event, the energies are transferred to atoms present in the host matrix.<sup>8</sup> Both ionization and elastic collision events affect the structures and properties of nuclear waste forms.<sup>8</sup>

Among the decay products,  $\alpha$ - and  $\beta$ - particles lose energy mainly by ionization processes while the recoil nuclei resulting from  $\alpha$ - and  $\beta$ - decay events transfer energy to atoms primarily via an elastic collision process.<sup>8</sup> The decay products resulting from  $\beta$ -decay do not possess enough energy (e.g., energy of  $\beta$ -particle ~ 0.5 MeV) to initiate atomic displacements in the host matrix.<sup>8</sup>

As a result,  $\beta$ -decay events do not cause significant damage to the structure of a nuclear wasteform.<sup>8</sup> However, the  $\alpha$ -decay event which produces high energy  $\alpha$ -particles (4.5 to 5.8 MeV) and  $\alpha$ -recoil atoms (70 to 100 keV) brings about the most structural damage in wasteforms.<sup>8</sup> During an  $\alpha$ -decay event, an  $\alpha$ -particle can travel over a range of 16 – 22  $\mu\text{m}$  and loses the majority of its energy to inducing ionization events.<sup>8</sup> A portion of the energy of an  $\alpha$ -particle is also used to produce a few hundred atomic displacements along its path with greater displacements occurring at the end of the particle trajectory.<sup>8</sup> The heavier  $\alpha$ -recoil atom, on the other hand, dissipates energy primarily via elastic collision processes over a very short range (30 – 40 nm) and causes 1000 to 2000 atomic displacements.<sup>8</sup> Compared to  $\alpha$ -recoil, the  $\beta$ -recoil atom only generates about 0.1 atomic displacements per  $\beta$ -decay event.<sup>8</sup> As a result, several studies have focused on investigating the radiation damage in solid waste forms due to  $\alpha$ -recoil atoms.<sup>11</sup>

The extent of structural damage due to  $\alpha$ -decay events varies depending on the dose (i.e., number of  $\alpha$ -decay events per gram of actinide) and type of nuclear waste form that is being studied.<sup>7</sup> Structurally, glass based host matrices in which atoms are arranged in a random fashion are less affected by the atomic rearrangements that occur as a result of  $\alpha$ -decay of actinides.<sup>7</sup> The minor changes in the structure of a glass that accompanies the radioactive decay of actinides are usually manifested in a small increase or decrease in the volume of a glass wasteform.<sup>7</sup> The maximum change in the volume of a glass waste form after  $\alpha$ -decay events is on the order of  $\sim 1\%$ .<sup>7</sup> As a result, significant changes in the chemical durability of glass waste forms are not observed after  $\alpha$ -decay. Crystalline waste forms, on the other hand, are structurally more affected by radiation damage events.<sup>7</sup> Crystalline materials are characterized by long-range periodic arrangement of atoms and, in the event of an  $\alpha$ -decay event, the high energy  $\alpha$ -recoil atom tends to disrupt this periodic arrangement either partially or completely.<sup>8</sup> In the former case, a disordered crystalline waste form is produced whereas in the latter the crystalline phase is completely transformed into an amorphous phase.<sup>8</sup> These structural changes are accompanied by a swelling of the waste form and the change in volume of the crystalline waste form can range between 5 % - 18%.<sup>8</sup> Swelling of a waste form results in an increase in its surface area thereby decreasing the chemical durability of crystalline wasteform.<sup>8</sup> The structural response of nuclear waste forms to  $\alpha$ -decay induced radiation damage events has been studied in the literature either via incorporation of actinides in a waste form (internal irradiation) and/or through simulation of damage by

implanting high energy charged particles in a waste form (external radiation).<sup>8,11</sup> A short account of internal and external irradiation methods is provided in the following section.

### **3.1. Internal Irradiation**

Radiation-induced structural damage due to  $\alpha$ -decay events is best studied through doping of short-lived actinides (e.g., Pu, Cm) in the waste form of interest.<sup>8,11</sup> In internal or self-irradiation methods, the radiation resulting from the  $\alpha$ -decay of incorporated actinides varies gradually with time and, accordingly, the structural performance of nuclear waste forms is monitored as a function of time. During an  $\alpha$ -decay event, the waste form is simultaneously exposed to radiation arising from both  $\alpha$ -particles and  $\alpha$ -recoil atoms.<sup>8</sup> Therefore, the internal irradiation method enables determination of structural stability of proposed waste forms under conditions that are quite similar to those experienced by HLW incorporated wastefoms.<sup>8</sup> However, the major disadvantages of employing an internal irradiation method to study radiation-induced damage process in waste forms are that it is time-consuming and the radioactivity of the waste form also places a limit on the access to various characterization techniques that could be used for examining the structure of the host matrix.<sup>11</sup>

### **3.2. External Irradiation**

The limitations faced by internal irradiation can be overcome using an external irradiation method in which the radiation events are simulated under laboratory conditions via high energy ion-implantation.<sup>8,11</sup> In this method, the radiation conditions representing different time periods of HLW storage is attained in a very short time by irradiating a thin region of the monolithic waste form (e.g., pellet) with high-energy ion beams (e.g.,  $\text{He}^{2+}$ ,  $\text{Ne}^+$ ,  $\text{Kr}^+$ ,  $\text{Au}^-$ ) of varying ion doses (i.e., number of ions/cm<sup>2</sup>).<sup>8,11</sup> The externally irradiated solids are also non-radioactive which therefore allows the use of different experimental techniques to characterize the ion-implanted solids.<sup>11</sup> Since  $\alpha$ -decay is the major decay pathway for actinides present in HLW, the waste forms are irradiated with high-energy light (e.g.,  $\text{He}^{2+}$ ) and/or heavy (e.g.,  $\text{Pb}^+$ ,  $\text{Au}^-$ ) ions to simulate radiation effects due to  $\alpha$ -particles and/or  $\alpha$ -recoil atoms (i.e., daughter products), respectively.<sup>12</sup>

## **4. Rare-earth phosphates as nuclear waste forms**

In the search for a suitable crystalline waste form, synthetic analogues of some of the naturally occurring rare-earth phosphate minerals have been identified as a potential host matrix for HLW storage.<sup>13</sup> The rare-earth phosphate minerals are both compositionally and structurally diverse and can be found in nature as monazite [(Ce,La,Nd,Th,U)PO<sub>4</sub>], xenotime [(Y,HREE,U,Th)PO<sub>4</sub>]; HREE

– heavy rare-earth elements], fluorapatite  $[(Ca,Ce)_5(PO_4)_3F]$ , vitusite  $[Na_3(Ce,La,Nd)(PO_4)_2]$ , rhabdophane  $[(Ce,La)PO_4.H_2O]$ , churchite  $[YPO_4.2H_2O]$ , and brockite  $[(Ca,Th,Ce)PO_4.H_2O]$ .<sup>14</sup> Of the various rare-earth phosphate minerals that exist in nature, the monazite and xenotime minerals contain the highest weight percent of rare-earth elements and these minerals are used commercially for the extraction of rare-earth elements.<sup>14</sup> Monazite and xenotime are abundant rare-earth minerals that exist as an accessory phase in rocks such as granitoids, rhyolites, and gneisses.<sup>14,15</sup> The mineral monazite is also found in alluvial deposits and beach sands as a result of the weathering of rocks.<sup>14,15</sup> In addition to accommodating rare-earth elements, the monazite and xenotime minerals also contain varying amounts of Th and U, which makes these minerals slightly radioactive.<sup>14</sup> Due to the presence of Th and U, these minerals have been exposed to radiation events over geological time scales and yet the monazite mineral, in particular, has not been found completely in a metamict state (i.e., amorphous).<sup>15</sup> This observation suggests that these minerals are structurally resistant to radiation damage events.<sup>15</sup> However, radiation studies on synthetic and natural monazite samples have shown that these minerals are easily damaged by radiation events but could also recover from structural damage upon annealing at lower temperatures.<sup>15</sup> Unlike the monazite mineral, radiation studies of xenotime minerals are not well documented in the literature. Monazite and xenotime minerals are also highly insoluble and possess high chemical durability in aqueous environments and this is demonstrated by the fact that the monazite minerals are still present in beach sands and placer deposits wherein the minerals are frequently exposed to aqueous conditions.<sup>15</sup> Based on this mineralogical evidence, synthetic analogues of monazite and xenotime minerals have been proposed as potential host candidates for nuclear waste sequestration applications.<sup>13,15</sup>

Another important mineral that is chemically related to monazite is rhabdophane.<sup>16</sup> Rhabdophane is a naturally occurring hydrous rare-earth phosphate mineral ( $REPO_4.nH_2O$ ; RE = La to Dy) that is formed during the aqueous alteration of monazite minerals and could play a role in controlling the solubility of actinides.<sup>16</sup> A few studies have shown the formation of rhabdophane on the surface of synthetic phosphate ceramics as a result of chemical alteration and have proposed that rhabdophane could act as a protective barrier by either delaying or stopping the release of actinides to the environment.<sup>16</sup> In terms of structural stability, the rhabdophane phase is considered to be stable at lower temperatures and can undergo structural transformations to the monazite- or xenotime- type structure at higher temperatures.<sup>16</sup> It is for this reason that the synthetic analogues

of the rhabdophane mineral have not received attention as a potential nuclear waste form in the literature.

A fourth polymorph of rare-earth phosphates referred to as churchite is also found in nature and like rhabdophane, churchite is also a hydrous rare-earth phosphate mineral ( $\text{REPO}_4 \cdot 2\text{H}_2\text{O}$ ; RE = Gd to Lu & Y).<sup>17</sup> Churchite-type materials lose water upon heating and eventually undergo a structural transformation to the xenotime-type structure.<sup>17</sup> It has been proposed that the churchite phase could precipitate on the surface of the xenotime mineral during the low temperature aqueous alteration of the latter and as a result, the churchite phase could play an important role in delaying or stopping the migration of actinides from the xenotime mineral to the biosphere.<sup>17</sup>

#### 4.1. Crystal Structures of Monazite and Xenotime

Monazite- ( $\text{REPO}_4$ ; RE = La to Gd) and Xenotime- ( $\text{RE}'\text{PO}_4$ ; RE = Tb to Lu & Y) type structures crystallize in monoclinic ( $P2_1/n$ ) and tetragonal ( $I4_1/amd$ ) crystal systems, respectively.<sup>18</sup> In the monazite structure, the RE ions are coordinated to nine oxygen atoms and the arrangement of oxygen atoms around the RE ion can be viewed as an equatorial pentagon of oxygen atoms interpenetrated by a tetrahedron of oxygen atoms (Figure 1.3a).<sup>18</sup> The  $\text{REO}_9$  polyhedra in the monazite structure consist of nine unique RE-O bond distances (e.g., Ce-O = 2.460 Å – 2.776 Å in  $\text{CePO}_4$ ) and, as a result, is significantly distorted. As a result of this distortion, the monazite structure offers greater structural flexibility and can accommodate cations of differing sizes and charges.<sup>8</sup> Chains of alternating  $\text{REO}_9$  polyhedra and  $\text{PO}_4$  tetrahedra connected via edge-sharing are present along the c-axis and these chains are connected to each other via edge-sharing of  $\text{REO}_9$  polyhedra (**Figure 2a**).

In the xenotime-type structure (e.g.,  $\text{YPO}_4$ ), the RE ions are coordinated to eight oxygen atoms and the resulting  $\text{REO}_8$  polyhedra consist of two unique RE-O bond distances (e.g., In  $\text{YPO}_4$ ,  $2 \times [4 \text{ Y-O}] = 2.309 \text{ \AA}$  and  $2.381 \text{ \AA}$ ; **Figure 2b**).<sup>18</sup> In comparison to the  $\text{REO}_9$  polyhedra in the monazite structure, the  $\text{REO}_8$  polyhedra in the xenotime structure are more symmetric and as a result, imposes size and charge restrictions on the cations that could be incorporated in the structure. Therefore, unlike the monazite structure, the xenotime structure is not expected to accommodate a wide variety of cations. Similar to the monazite structure, edge-sharing chains of  $\text{REO}_8$  and  $\text{PO}_4$  polyhedra are present along the c-axis and these chains are connected to each other through edge-sharing of  $\text{REO}_8$  polyhedra (Figure 1.3b).<sup>18</sup>

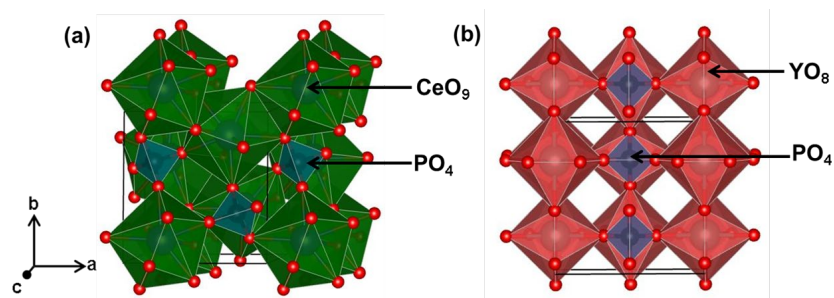


**Figure 2** Crystal structures of (a)  $\text{CePO}_4$  (Monazite-type; Space group:  $P2_1/n$ ) and (b)  $\text{YPO}_4$  (Xenotime-type; Space group:  $I4_1/amd$ ).

## 4.2. Crystal Structure of Rhabdophane

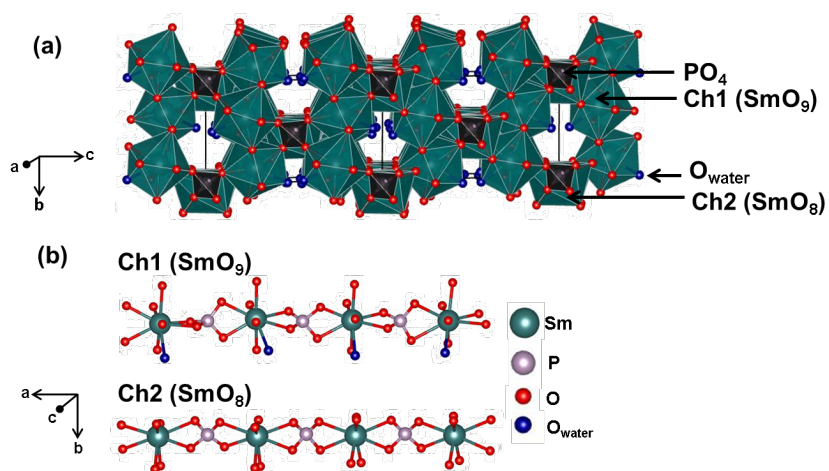


**Figure 3** (a) Crystal structure of  $\text{SmPO}_4 \cdot 0.667\text{H}_2\text{O}$  (rhabdophane-type; Space group:  $C2$ ). (b) Ball and stick representation of the alternate arrangement of Sm and P atoms in chains 1 (Ch1) and 2 (Ch2). Reprinted with permission from Reference <sup>19</sup> (Rafiuddin and Grosvenor *Inorg. Chem* 2016, 55, 9685-9695). Copyright 2016 American Chemical Society

Rhabdophane ( $\text{SmPO}_4 \cdot 2\text{H}_2\text{O}$ ) materials crystallize in a monoclinic crystal system (Space group:  $C2$ ) and the crystal structure consist of two chains (Ch1 and Ch2) of alternating Sm-O polyhedra and  $\text{PO}_4$  tetrahedra (**Figure 3a**).<sup>16</sup> All the  $\text{PO}_4$  tetrahedra in Ch1 (**Figure 3b**) are distorted to the same extent and have four unique P-O bond distances and P-O-P bond angles whereas in Ch2, the symmetry of the alternating  $\text{PO}_4$  tetrahedra are not the same (i.e., four unique P-O bond distances and P-O-P bond angles in the first  $\text{PO}_4$  tetrahedra followed by two unique P-O bond distances and P-O-P bond angles in the second  $\text{PO}_4$  tetrahedra).<sup>16,19</sup> The Sm ion in Ch1 is

coordinated to nine O atoms with eight O atoms provided by PO<sub>4</sub> tetrahedra and the remaining one O atom arising from water (**Figure 3b**).<sup>16</sup> In Ch2, the Sm ion is coordinated to eight O atoms.<sup>16</sup> The connection of Ch1 and Ch2 results in the formation of open channels along the ‘a’ direction and the water molecules occupy these open channels (**Figure 3a**).<sup>16</sup>

### 4.3. Crystal Structure of Churchite

The churchite- (YPO<sub>4</sub>.2H<sub>2</sub>O) type structure is isostructural to the gypsum (CaSO<sub>4</sub>.2H<sub>2</sub>O) structure and crystallizes in a monoclinic crystal system (Space group – C2/c).<sup>20</sup> The crystal structure of YPO<sub>4</sub>.2H<sub>2</sub>O comprises of 2D layers of YO<sub>8</sub> and PO<sub>4</sub> polyhedra and these layers are stacked along the ‘b’ direction (**Figure 4**). Within each layer, 1D chains of alternating YO<sub>8</sub> and PO<sub>4</sub> polyhedra are connected via edge-sharing of the PO<sub>4</sub> tetrahedra and these 1D chains are in turn connected to each other via edge-sharing of the YO<sub>8</sub> polyhedra. In the YO<sub>8</sub> polyhedra, the central yttrium atom is bonded to eight oxygen atoms of which six oxygen atoms are provided by the neighboring phosphate groups and the remaining two oxygen atoms are provided by the water molecules.<sup>20</sup> The YO<sub>8</sub> polyhedra adopts a distorted square antiprism geometry and the Y-O bond distances in this polyhedra ranges from 2.29 Å to 2.48 Å.<sup>20</sup> The longest Y-O bond distances are attributed to the bidentate bonding with the neighbouring phosphate groups.<sup>20</sup> In the PO<sub>4</sub> tetrahedra, the P-O bond distances are 1.53 Å and 1.52 Å and are typical of an orthophosphate anion.<sup>20</sup> However, the bond angles in the PO<sub>4</sub> tetrahedra exhibit a deviation from the ideal geometry thereby indicating that the PO<sub>4</sub> tetrahedra are distorted.<sup>20</sup> The 2D layers of the churchite structure are held together through the formation of hydrogen bonds (H-bond) between the layers and this results in the formation of a 3D network.<sup>20</sup> In addition to the inter-layer H-bonds, intra-layer H-bonds are also present in the churchite-type structure.

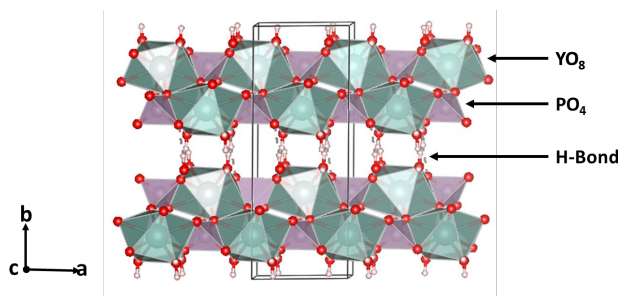


**Figure 4** Crystal structure of churchite-type YPO<sub>4</sub>.2H<sub>2</sub>O. The dotted lines in the interlayer region represent the H-bond.

### 5. Effect of Ion-irradiation on the structure of REPO<sub>4</sub>

Numerous studies have employed an external irradiation method to investigate the effect of radiation on the structures of REPO<sub>4</sub> materials.<sup>21,22</sup> In the external irradiation method, single or dual ion-beam irradiation of REPO<sub>4</sub> has been performed followed by analysis using a variety of techniques. In single ion-beam irradiation mode, heavy or light ion beams such as Au or He are typically used for ion-irradiation and simulate the structural changes due to either  $\alpha$ -recoil atom or  $\alpha$ -particle. In dual ion-beam irradiation mode, heavy and light ion beams such as Au and He are used in tandem, respectively. Dual ion-beam irradiation simulates the combined effects of  $\alpha$ -recoil atom and  $\alpha$ -particle on the structure of REPO<sub>4</sub>. The structural response of REPO<sub>4</sub> ceramics to ion-irradiation has been studied using various structural characterization techniques such as in-situ Transmission Electron Microscopy (TEM), Glancing angle X-ray absorption near edge spectroscopy (GA-XANES), Photoluminescence spectroscopy etc.<sup>12,21,22</sup> Two independent studies investigating the effect of ion-irradiation on the structure of REPO<sub>4</sub> using ex-situ GA-XANES and in-situ TEM techniques will be discussed in the following sections.<sup>12,22</sup>

### **5.1. A GA-XANES investigation of ion-irradiated REPO<sub>4</sub> ceramics**

Rafiuddin and Grosvenor investigated the structural response of Au<sup>-</sup> ion irradiated La<sub>1-x</sub>Yb<sub>x</sub>PO<sub>4</sub> ceramics using GA-XANES.<sup>22</sup> The La<sub>1-x</sub>Yb<sub>x</sub>PO<sub>4</sub> (x = 0.0, 0.3, 0.7, 1.0) ceramics were synthesized by conventional solid-state methods and sintered pellets were produced prior to Au<sup>-</sup> ion-implantation. In that study, high energy Au<sup>-</sup> ions (2 MeV) of varying ion doses ( $1 \times 10^{14}$ ,  $5 \times 10^{14}$ , and  $1 \times 10^{15}$  ions/cm<sup>2</sup>) were implanted into La<sub>1-x</sub>Yb<sub>x</sub>PO<sub>4</sub> pellets.<sup>22</sup> A Stopping and Range of Ions in Matter (SRIM- 2013) software package was used in this study to generate the Au<sup>-</sup> ion implantation depth profile in La<sub>1-x</sub>Yb<sub>x</sub>PO<sub>4</sub>. SRIM calculations have shown that the Au<sup>-</sup> ions were implanted to a depth ranging between 50 nm – 450 nm and that the maximum number of Au<sup>-</sup> ions was found at a depth of ~275 nm. Since the ions are implanted in the near-surface region of the pellet, a surface sensitive GA-XANES technique was used in this study to monitor the changes in the local structure of the material due to ion-implantation. The local structure around the P atom in ion-irradiated La<sub>1-x</sub>Yb<sub>x</sub>PO<sub>4</sub> ceramics was investigated using P K-edge GA-XANES. The P K-edge GA-XANES spectra of ion-irradiated LaPO<sub>4</sub> (monazite-type) and YbPO<sub>4</sub> (xenotime-type) ceramics are shown in **Figure 5** and **Figure 6**.<sup>22</sup> In comparison to the pristine as-synthesized material, the P K-edge GA-XANES spectra of ion-irradiated LaPO<sub>4</sub> and YbPO<sub>4</sub> exhibited significant changes in the near-edge lineshape thus indicating a change in the local structure of P due to ion-implantation. In this study, the change in the local structure of P was attributed to a

distortion of the PO<sub>4</sub> tetrahedra caused by ion implantation.<sup>22</sup> It was observed in this study that for YbPO<sub>4</sub> ceramics implanted to a dose of  $1 \times 10^{15}$  ions/cm<sup>2</sup>, the spectral lineshape of the ion irradiated material showed similarities to the pristine material thus indicating a partial recrystallization of the structure.<sup>22</sup> It was proposed in this study that the partial recrystallization could be a result of the high dose of Au<sup>-</sup> ions causing a local heating of the sample and, thus, providing the necessary impetus for the movement of some of the displaced atoms to their original lattice sites.<sup>22</sup>

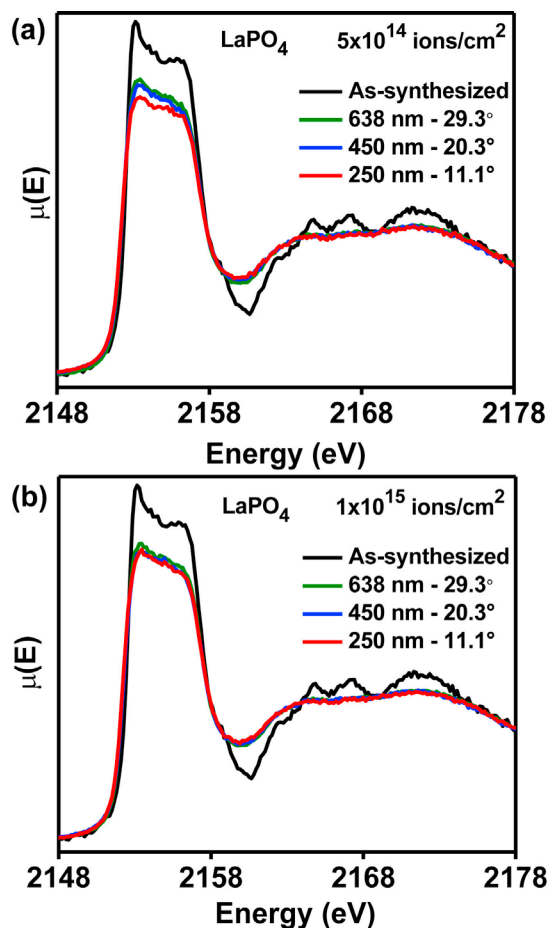


**Figure 5** P K-edge GA-XANES spectra of LaPO<sub>4</sub> implanted with Au<sup>2-</sup> ions to doses of a)  $5 \times 10^{14}$  ions/cm<sup>2</sup> and b)  $1 \times 10^{15}$  ions/cm<sup>2</sup>. Reprinted with permission from Reference <sup>22</sup> (Rafiuddin and Grosvenor *J. Alloys Compd.* 2015, 653, 279-289). Copyright 2015 Elsevier B.V.

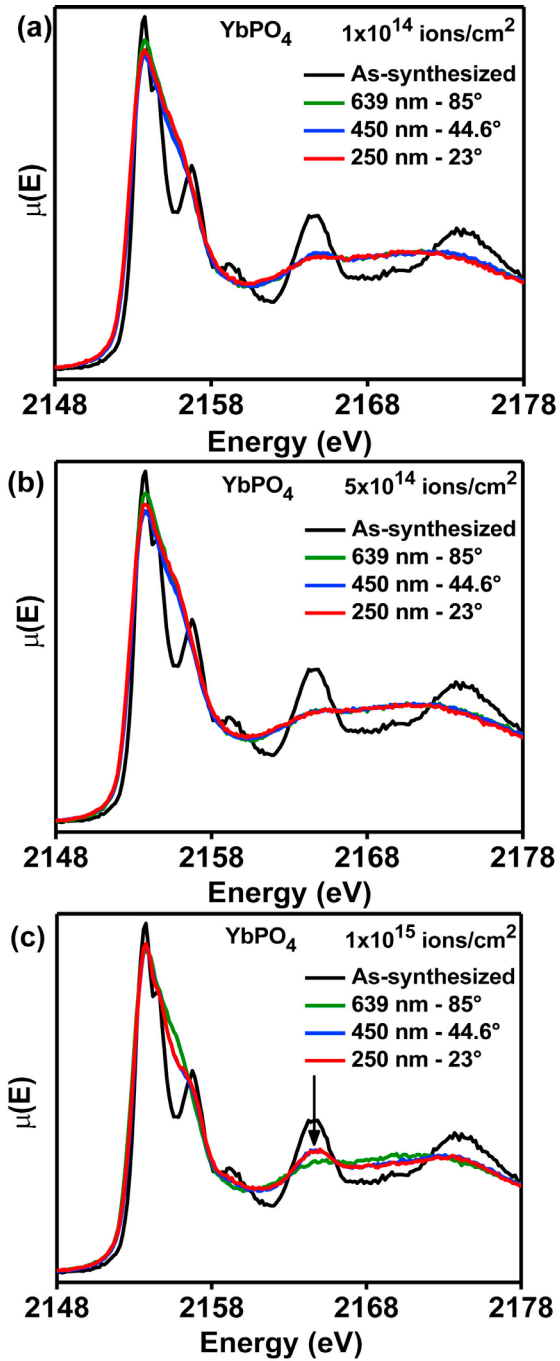


**Figure 6** P K-edge GA-XANES spectra of YbPO<sub>4</sub> implanted with Au<sup>2+</sup> ions to doses of a)  $1 \times 10^{14}$  ions/cm<sup>2</sup>, b)  $5 \times 10^{14}$  ions/cm<sup>2</sup>, and b)  $1 \times 10^{15}$  ions/cm<sup>2</sup>. Reprinted with permission from Reference <sup>22</sup> (Rafiuddin and Grosvenor *J. Alloys Compd.* 2015, 653, 279-289). Copyright 2015 Elsevier B.V.

The effect of annealing on the structure of ion-irradiated  $\text{La}_{1-x}\text{Yb}_x\text{PO}_4$  was also investigated in this study to determine if the materials could recover from the structural damage via thermal annealing.<sup>22</sup> Ion irradiated  $\text{La}_{1-x}\text{Yb}_x\text{PO}_4$  samples were heated to 300°C and 900°C and the structural response was monitored using P K-edge GA-XANES (**Figure 7**).<sup>22</sup> Evidence of partial structure recovery was observed for all samples annealed to 300°C as indicated by the similarities in the spectral lineshape of the ion-irradiated sample to those of the pristine material. Similar observations were made in this study for  $\text{LaPO}_4$ ,  $\text{La}_{0.7}\text{Yb}_{0.3}\text{PO}_4$ , and  $\text{La}_{0.3}\text{Yb}_{0.7}\text{PO}_4$  annealed to 900 °C though complete structural recovery was only observed for the  $\text{YbPO}_4$  sample annealed to 900 °C.<sup>22</sup>

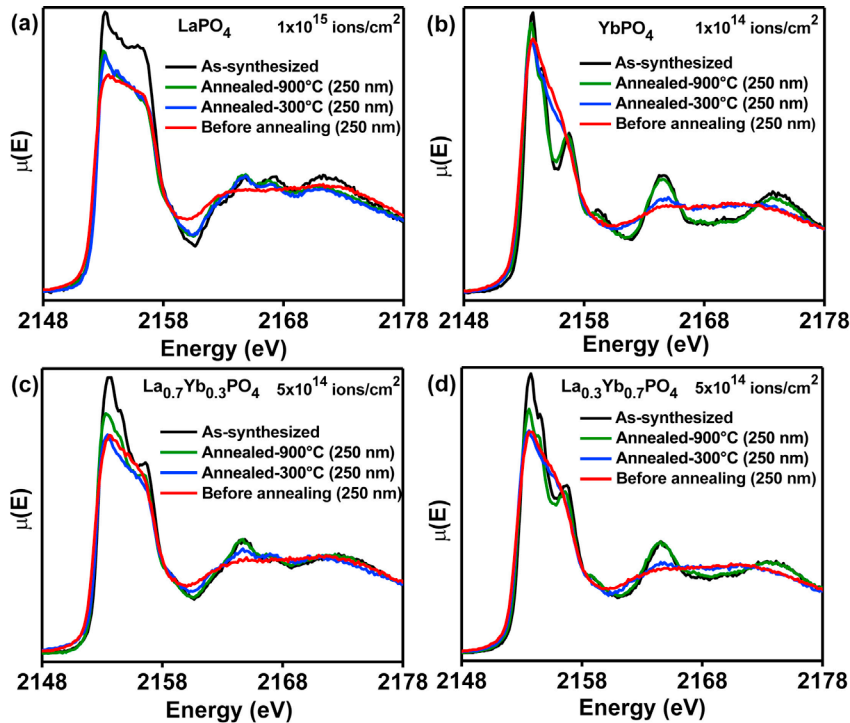


**Figure 7** P K-edge GA-XANES spectra of  $\text{Au}^{2+}$  ion implanted a)  $\text{LaPO}_4$ , b)  $\text{YbPO}_4$ , c)  $\text{La}_{0.7}\text{Yb}_{0.3}\text{PO}_4$ , and d)  $\text{La}_{0.3}\text{Yb}_{0.7}\text{PO}_4$  annealed to 300°C and 900°C. Reprinted with permission from Reference <sup>22</sup> (Rafiuddin and Grosvenor *J. Alloys Compd.* 2015, 653, 279-289). Copyright 2015 Elsevier B.V.

## 5.2. An in-situ TEM investigation of dual ion-beam irradiated $\text{REPO}_4$ ceramics

Rafiuddin et al. investigated the effect of dual ion beam irradiation on the structure of xenotime-type ErPO<sub>4</sub> ceramics using *in-situ* TEM.<sup>12</sup> In this study, the ErPO<sub>4</sub> powders were synthesized via a hydrothermal method and the resulting powders were pressed into pellets of 5 mm diameter and sintered at 1600°C in air for 3 h. Prior to ion irradiation, a Focused Ion Beam (FIB) technique was used to prepare thin lamellas of ErPO<sub>4</sub> (Dimension  $\sim 10.30 \times 5.40$   $\mu\text{m}$ ; Thickness  $\sim 60 - 83$  nm). In this study, the dual ion beam irradiation was performed under *in-situ* conditions inside a 200 keV TEM vacuum chamber and the structural response was monitored using *in-situ* TEM.<sup>12</sup> The ErPO<sub>4</sub> lamellas were irradiated using 1.5 MeV Au<sup>2+</sup> and 160 keV He<sup>+</sup> ions in sequential and simultaneous irradiation modes.<sup>12</sup> In the sequential mode, the lamellas were first irradiated using Au<sup>2+</sup> ions followed by irradiation using He<sup>+</sup> ions whereas in the simultaneous mode the lamellas were irradiated simultaneously using both Au<sup>2+</sup> and He<sup>+</sup> ions.

It was shown in this study that the xenotime-type ErPO<sub>4</sub> material turned amorphous upon irradiation with Au<sup>2+</sup> ions at a fluence of  $5 \times 10^{13}$  ions/cm<sup>2</sup> (**Figure 8**).<sup>12</sup> Sequential irradiation of the amorphous lamella with He<sup>+</sup> ions ( $1 \times 10^{17}$  ions/cm<sup>2</sup>) did not result in the recrystallization of the sample.<sup>12</sup> However, simultaneous irradiation (Au<sup>2+</sup>+ He<sup>+</sup>) of the ErPO<sub>4</sub> material did not result in radiation-induced amorphization of the sample at all the ion-fluences studied and the material continued to remain crystalline (**Figure 9**).<sup>12</sup> An  $\alpha$ -healing mechanism (i.e., healing of structural defects due to the rise in the local temperature of the material occurring as a result of  $\alpha$ -particle irradiation, ionization-driven diffusion of point defects, and recombination of vacancy and interstitial sites) was proposed in this study to explain the absence of radiation-induced amorphization.<sup>12</sup>

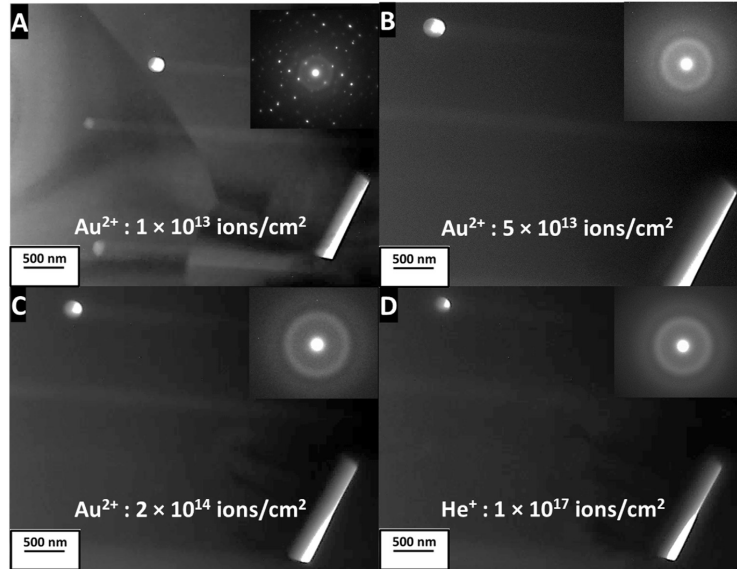


**Figure 8** TEM images and Selected area electron diffraction patterns of  $\text{ErPO}_4$  samples irradiated with  $\text{Au}^{2+}$  ions to fluences of  $1 \times 10^{13}$  ions/cm<sup>2</sup> (A),  $5 \times 10^{13}$  ions/cm<sup>2</sup> (B), and  $2 \times 10^{14}$  ions/cm<sup>2</sup> (C). TEM image and SAED pattern of amorphous  $\text{ErPO}_4$  irradiated with  $\text{He}^+$  ions to a fluence of  $1 \times 10^{17}$  ions/cm<sup>2</sup> (D). Reprinted with permission from Reference <sup>12</sup> (Rafiuddin et al. J. Nucl. Mater. 2020, 539, 152265). Copyright 2020 Elsevier B.V.

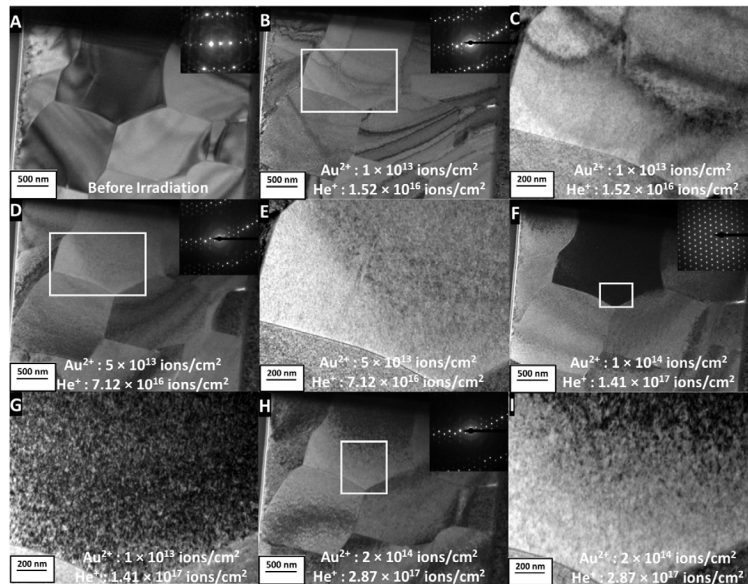


**Figure 9** TEM images and SAED patterns of pristine  $\text{ErPO}_4$  (A) and dual ion beam ( $\text{Au}^{2+} + \text{He}^+$ ) irradiated  $\text{ErPO}_4$  (B - I). Reprinted with permission from Reference <sup>12</sup> (Rafiuddin et al. J. Nucl. Mater. 2020, 539, 152265). Copyright 2020 Elsevier B.V.

## 6. Glass-REPO<sub>4</sub> composites

As indicated earlier, glass-ceramic composites have been proposed as next-generation materials for nuclear waste sequestration applications. Glass-ceramic composite materials are

normally synthesized using a two-step process where the ceramic and glass phases are synthesized separately before being mixed and then annealed to form a composite material.<sup>23</sup> A one-step method has been investigated where all precursors are mixed from the beginning followed by annealing. A one-step method would save on fabrication costs and would be compatible with already existing glass producing infrastructure and would also be safer since the HLW would not need to be handled for as long a period compared to the two-step method. Glass-ceramic composites containing  $\text{LaPO}_4$  (monazite-type),  $\text{YPO}_4$  (xenotime-type) or  $\text{CePO}_4$  (xenotime-type) crystallites dispersed in a borosilicate glass matrix have been synthesized by both 1- and 2-step methods using either solid-state or co-precipitation methods.<sup>23–25</sup> It was observed that glass-ceramic composites containing rare-earth phosphates dispersed in a borosilicate glass matrix could be formed using either 1- or 2-step methods and exhibit similar properties (e.g., morphology, crystal structures, etc.).<sup>23</sup> However, when comparing the solid-state vs. co-precipitation methods, it was observed that these glass-ceramic composite materials could be formed at significantly lower temperatures when using the co-precipitation method (e.g., 700 °C) compared to the solid-state method (e.g., 1100 °C).<sup>24,25</sup> Further, it was also demonstrated that the glass-composition can affect the formation of secondary (i.e., unwanted) crystalline phases when lower annealing temperatures were used.<sup>24</sup> An example SEM image and corresponding EDX maps from a glass-ceramic composite material containing  $\text{CePO}_4$  crystallites formed by a 1-step co-precipitation method are shown in **Figure 10**.<sup>25</sup>

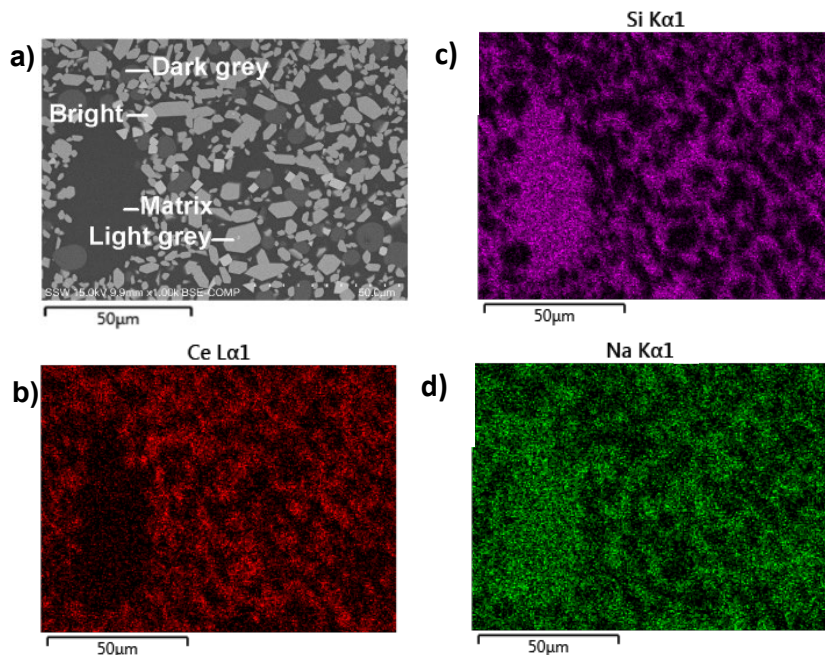


**Figure 10** SEM image of 40 wt% CePO<sub>4</sub>-BG composite material synthesized with a Ce<sup>4+</sup> precursor and annealed at 1100 °C, EDX maps of b) Ce, c) Si, and d) Na. Reprinted with permission from Reference <sup>25</sup> (Donato and Grosvenor *Cryst. Growth Des.* 2020, 20, 2217 -2231)

## 7. Summary and conclusions

Several strategies have been proposed for the safe sequestration of nuclear waste, which is important for the continued expansion of nuclear power plants to help combat climate change. While this article has focussed on rare-earth phosphate materials, it should be noted that many solid-state materials having different structures and compositions have been proposed for the sequestration of nuclear waste. Rare-earth phosphates are an interesting class of solid-state materials owing to the variety of structures that can be adopted and various compositions. These materials are promising nuclear waste forms owing to their ability to accommodate a range of rare-earth and actinide ions; however, further work is required. This includes studying the corrosion resistance of these materials, which has already begun, and studying their ability to accommodate HLW elements such as minor actinides. It is also believed that composite materials will be important waste form materials owing to the ability of these materials to incorporate a broad range of nuclear waste elements.

## Acknowledgements

The Natural Sciences and Engineering Research Council (NSERC) of Canada funded this project through a discovery grant awarded to APG. MRR and AM would also like to thank the French National Research Agency (ANR JCJC-X-MAS; Project # ANR17-CE06-0004) for the financial support. MRR also thanks the Engineering and Physical Sciences Research Council for funding under grants, EP/T012811/1.

## References

- (1) *The Canadian Nuclear Factbook*; Canadian Nuclear Association, 2020.
- (2) *Nuclear Energy Outlook*; Nuclear Energy Agency, 2008.
- (3) *National Inventories and Management Strategies for Spent Nuclear Fuel and Radioactive Waste - Methodology for Common Presentation of Data*; Nuclear Energy Agency, 2016.
- (4) Ojovan, M. I.; Burakov, B. E.; Lee, W. E. Radiation-induced microcrystal shape change as a mechanism of wastefrom degradation. *J. Nucl. Mater.* **2018**, *501*, 162–171.
- (5) Lee, W. E.; Ojovan, M. I.; Stennett, M. C.; Hyatt, N. C. Immobilization of radioactive waste in glasses, glass composite materials and ceramics. *Adv. Appl. Ceram.* **2006**, *105* (1), 3–12.
- (6) Donald, I.; Metcalfe, B. L.; Taylor, R. N. J. The immobilization of high level radioactive wastes using ceramics and glasses. *J. Mater. Sci.* **1997**, *32* (22), 5851–5887.
- (7) Weber, W. J.; Navrotsky, A.; Stefanovsky, S.; Vance, E. R.; Vernaz, E. Material science of high-level nuclear waste immobilization. *MRS Bull.* **2009**, *34* (1), 46–53.
- (8) Weber, W. J.; Ewing, R. C.; Catlow, C. R. A.; de la Rubia, T. D.; Hobbs, L. W.; Kinoshita, C.; Matzke, H.; Motta, A. T.; Nastasi, M.; Salje, E. K. H.; Vance, E. R.; Zinkle, S. J. Radiation effects in crystalline ceramics for the immobilization of high-level nuclear waste and plutonium. *J. Mater. Res.* **1998**, *13* (06), 1434–1484.
- (9) McCloy, J. S.; Schuller, S. Vitrification of wastes: from unwanted to controlled crystallization, a review. *Comptes Rendus. Géoscience* **2022**.
- (10) Deng, Y.; Liao, Q.; Wang, F.; Zhu, H. Synthesis and characterization of cerium containing iron phosphate based glass-ceramics. *J. Nucl. Mater.* **2018**, *499*, 410–418.
- (11) Yudinsev, S. V.; Lizin, A. a.; Livshits, T. S.; Stefanovsky, S. V.; Tomilin, S. V.; Ewing, R. C. Ion-beam irradiation and <sup>244</sup>Cm-doping investigations of the radiation response of actinide-bearing crystalline waste forms. *J. Mater. Res.* **2015**, *7* (May), 1–13.
- (12) Rafiuddin, M. R.; Seydoux-Guillaume, A.-M.; Deschanel, X.; Mesbah, A.; Baumier, C.; Szenknect, S.; Dacheux, N. An in-situ electron microscopy study of dual ion-beam irradiated xenotime-type ErPO<sub>4</sub>. *J. Nucl. Mater.* **2020**, *539*, 152265.
- (13) Oelkers, E. H.; Montel, J.-M. Phosphates and nuclear waste storage. *Elem.* **2008**, *4* (2), 113–116.
- (14) Long, K. R.; Van Gosen, B. S.; Foley, N. K.; Cordier, D. *The principal rare earth elements deposits of the United States - A summary of domestic deposits and a global perspective: U.S. Geological Survey Scientific Investigations Report 2010-5220*; 2010.
- (15) Boatner, L. A. Synthesis, structure, and properties of monazite, pretulite, and xenotime. *Rev. Mineral. Geochemistry* **2002**, *48* (1), 87–121.
- (16) Mesbah, A.; Clavier, N.; Elkaim, E.; Gausse, C.; Kacem, I. Ben; Szenknect, S.; Dacheux, N. Monoclinic form of the rhabdophane compounds: REEPO<sub>4</sub>·0.667H<sub>2</sub>O. *Cryst. Growth Des.* **2014**, *14* (10), 5090–5098.
- (17) Subramani, T.; Rafiuddin, M. R.; Shelyug, A.; Ushakov, S.; Mesbah, A.; Clavier, N.; Qin, D.; Szenknect, S.; Elkaim, E.; Dacheux, N.; Navrotsky, A. Synthesis, crystal structure and enthalpies of formation of churchite-type REPO<sub>4</sub>·2H<sub>2</sub>O (RE = Gd to Lu) materials. *Cryst. Growth Des.* **2019**, *19* (8), 4641–4649.
- (18) Ni, Y.; Hughes, J. M.; Mariano, A. N. Crystal chemistry of the monazite and xenotime structures. *Am. Mineral.* **1995**, *80*, 21–26.
- (19) Rafiuddin, M. R.; Grosvenor, A. P. A structural investigation of hydrous and anhydrous

- rare-earth phosphates. *Inorg. Chem.* **2016**, *55* (19), 9685–9695.
- (20) Ivashkevich, L. S.; Lyakhov, A. S.; Selevich, A. F. Preparation and structure of the yttrium phosphate dihydrate. *Phosphorus Res. Bull.* **2013**, *28* (3), 45–50.
- (21) Lenz, C.; Thorogood, G.; Aughterson, R.; Ionescu, M.; Gregg, D. J.; Davis, J.; Lumpkin, G. R. The quantification of radiation damage in orthophosphates using confocal  $\mu$ -luminescence spectroscopy of  $\text{Nd}^{3+}$ . *Front. Chem.* **2019**, *7*, 13.
- (22) Rafiuddin, M. R.; Grosvenor, A. P. Probing the effect of radiation damage on the structure of rare-earth phosphates. *J. Alloys Compd.* **2015**, 653.
- (23) Donato, G.; Holzschere, D.; Beam, J. C.; Grosvenor, A. P. A one-step synthesis of rare-earth phosphate-borosilicate glass composites. *RSC Adv.* **2018**, *8* (68), 39053–39065.
- (24) Donato, G.; Grosvenor, A. P. Effect of glass composition on the crystallization of  $\text{CePO}_4$ -borosilicate glass composite materials. *Can. J. Chem.* **2020**, *98* (11), 701–707.
- (25) Donato, G.; Grosvenor, A. P. Crystallization of rare-earth phosphate -borosilicate glass composites synthesized by a one-step coprecipitation method. *Cryst. Growth Des.* **2020**, *20* (4), 2217–2231.